https://doi.org/10.48048/tis.2022.6179

The Development Study of the Drag Coefficient of Solid Cylinder on Inclined Plane in Water

Reza Ariefka[1,*] and Yudhiakto Pramudya[2]

[1]STKIP Muhammadiyah OKU Timur, Sumatera Selatan 32382, Indonesia
[2]Program Studi Magister Pendidikan Fisika, Universitas Ahmad Dahlan, Yogyakarta 55166, Indonesia

([*]Corresponding author's-email: rezaariefka@gmail.com)

Received: 14 July 2021, Revised: 29 September 2021, Accepted: 6 October 2021

Abstract

The dynamic resistance of a fluid to a cylinder rolling on an inclined plane in water has been experimentally studied. This creates problems in the form of solid-liquid interactions, which include landslides on the seabed and debris flows on the seabed that cause Tsunamis. The development of flow around a rolling cylinder is described to highlight the implications on the nature of the hydrodynamic force coefficient acting on the cylinder as resistance. The coefficient of drag on the cylinder when rolling on an inclined plane in water is the coefficient of drag that prevents the cylinder from rolling. In addition, other external force coefficients (besides the drag coefficient) also impede the cylinder motion. The equation of motion of the cylinder is solved with experimental data which is used as the most suitable solution to get the drag coefficient value. The movement of the cylinder is also not perfectly linear because there is a force from the side of the track and the cylinder moves slightly zigzag in 1-D motion.

Keywords: Drag coefficients, Rolling cylinder, Mass coefficients, Reynolds number, Logger pro

Introduction

Research has been carried out on determining the Drag Coefficient of motion of a ball material on an inclined plane in the water, it is found that the drag force on the motion of the ball when rolling is always greater than that of a free-falling ball under all kinematic conditions, although some of the Reynolds number values increase [1]. In addition to spherical materials, the science of friction (drag) fluid dynamics in cylinder material is very rare and very much needed when designing the measurement process for a particular cylindrical material particles system [2,3]. Thus, there is a lot of information available in the literature for the estimation of drag on cylindrical particles [4,5]. Most of this information, however, relates to when the cylinder is at rest with the fluid moving or when the cylinder is moving with the fluid at rest. In both conditions, the cylinder does not come into contact with the solid surface boundary [6-12]. Many state particles roll, with or without shear motion in the fluid. The most common example is flow in a rolling ball viscometer provided it measures the rolling speed of the ball very accurately on an inclined plane in the tube; Hydraulic transport of solid particles on inclined pipes also causes particles to roll along the pipe walls, especially when the pipe is operating in a moving system. Other examples are landslides on the seabed on mountain slopes, flow of shale material on the seabed, sediment transport on the coast, movement of seabed gravel due to ocean currents.

Landslides can cause tsunamis if the most critical mountain slope angles in the sea are at the edge of the shelf. If the slopes of this mountain are in the area of the earthquake path, it is very easy for landslides to occur (flank collapse) on the slopes of the mountain if there are disturbing vibrations. That is why an earthquake with a small force can trigger an avalanche that will cause a tsunami. The volume of landslide debris material, the process of movement of the landslide debris material and the slope of the mountain slopes are the parameters that most influence the characteristics of the tsunami. The steeper slopes of the mountains will cause landslides to move faster into the water, causing high water waves in the form of tsunamis [13-30]. The high number of deaths from these events is related to the limited literature on tsunami generation from mechanisms other than fault damage and the lack of an effective tsunami warning system for non-seismic events [31]. However, before the description of this study, previous research related to this study will be described.

Research related to this field is the determination of viscosity using a rolling ball viscometer and the law of fluid power [32,33]. Theoretically, the lubrication flow approach is applied to the thin gap between the sphere and the tube wall to extract dynamic viscosity values from Newtonian medium and the law of constant force for non-Newtonian fluids. The device is calibrated with a fluid whose viscosity value is known and a working equation that relates the viscosity kinematics to the last time the ball rolled (a certain tube-ball combination) with a fixed distance. In principle, the data can be converted into a Reynold coordinate drag coefficient. Hasan [34], carried out measurements of the wall effect on the velocity of the ball when rolling on Newtonian fluid, obtained (d/D) > 0.707, for the value of the product (C_dR_e) hardly depends on the value of the Reynold number.

Another study of the rotating motion of the ball relates to open canals [35]. In the flow in the tube, the wall exerts an extra retardation effect on the ball, which is caused by the upward movement of the fluid through the eccentric ring gap between the ball and the tube wall, this effect is usually neglected for the ball rolling in. open channel geometry. From the description above, it can be concluded that the dynamic resistance of the fluid on a ball rolling on Newtonian fluid is little known on the tube walls which tend to be slippery. In addition, Ariefka and Pramudya [36] have conducted research on the study of hollow cylinders in an inclined plane to determine the moment of inertia of the cylinder with variations in plane trajectory distance and plane tilt angle. The value of the moment of inertia of the experiment for the distance and angle variation obtained is influenced by the diameter of the cylinder bore.

This research aims to determine the drag coefficient of cylindrical material motion on an inclined plane in water experimentally as a function of the slope angle. This information is used to develop universal position-time and velocity-time relationships. There are many rational understandings of the state of the fluid dynamics drag coefficient in cylindrical rolling motion that can be used to develop realistic models of complex processes, such as the drag coefficients of landslide materials in the seabed and the flow of debris on the seabed that causes a tsunami. This aims to add to the research literature on drag coefficients and as mitigation of large non-tectonic tsunamis due to seabed landslides in Indonesia in the future.

Theory

The previous paper presents the results of research on determining the coefficient of drag of the ball experimentally where the effect of the trajectory of the ball in the form of a tube causes an increase in the value of the drag coefficient with an average deviation of 8 - 20 % [1]. Due to the significant deviation of the drag coefficient, it is necessary to develop another material in the form of a cylinder that rolls on an inclined plane in the water, related to the determination of the drag coefficient experimentally, besides the availability of variations of solid ball materials that are difficult to obtain. The cylinder rolls down an inclined plane in stationary water due to its own gravity, the force acting on the cylinder is the drag force of the fluid F_D, the lift fluid F_L, the buoyancy force of the cylinder $F_B = mg\sin\theta$ and the resulting resistance force to wind F_R. All the forces are shown schematically in **Figure 1**.

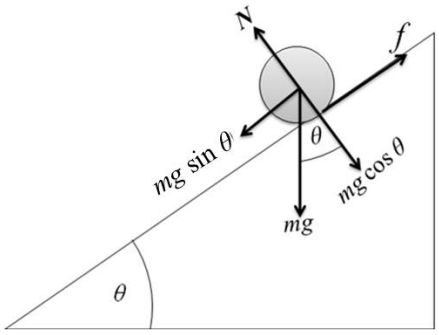

Figure 1 Force on a cylinder rolling on inclined plane in water.

In a state of equilibrium, when the cylinder is not experiencing acceleration and without a significant effect due to lift, the direction of the balancing force is the result of motion [37,38]:

$$F_D + F_R = mg\sin\theta \quad (1)$$

Where the fluid-drag force F_D can be expressed as the drag coefficient C_D which is defined as [39-521]:

$$F_D = \frac{1}{2} C_D \rho_f v_T{}^2 A \tag{2}$$

$A = PL = Pd$ is the surface area of the cylinder. Because the mass $m = \rho V$ and the volume of the cylinder $V = \pi R^2 t = \pi R^2 L$ then Eq. (2) becomes:

$$C_D = \frac{2\pi R^2 L}{v_T{}^2 Pd} \frac{\left(\rho_s - \rho_f\right)}{\rho_f} g \sin\theta \tag{3}$$

Or:

$$v_T{}^2 = \frac{2\pi R^2 L}{C_D Pd} \frac{\left(\rho_s - \rho_f\right)}{\rho_f} g \sin\theta \tag{4}$$

With C_D is the coefficient of drag, v_T is the terminal velocity, L is the height of the cylinder, P is the length of the cylinder, R is the cylinder radius for all the same materials, d is the cylinder diameter for all materials of the same value, ρ_s is the density of the cylinder, ρ_f = 1,000 kg/m^3 is the density of the fluid (water), g = 9.8 m/s^2 is the gravitational acceleration of the earth, and θ is the angle of inclination of the track. Long value P cylinder = high L cylinder, width value l cylinder = diameter d cylinder. The interaction between cylinder and fluid is influenced by Reynold's number which identifies the type of flow (laminar or turbulence), laminar flow is a fluid motion in which each particle in the fluid follows the same path as the previous particle, characterized by a smooth or regular trajectory of the fluid particles. Laminar flow occurs at Reynold's number less than 3×10^5 [53]. Then the equation for Reynold's number R_e is [54-58]:

$$R_e = \frac{\rho v d}{\mu} \tag{5}$$

Where ρ is the density of the fluid (water), v is the cylinder speed, d is the cylinder diameter, μ = 0.001 is the viscosity of water.

Materials and methods

Materials

In this study, using an aquarium measuring 1.30×0.50×0.55 m, 1.20 m inclined track board, 4 cylinders (brass, stainless steel, iron and aluminum) with the same height height $L = (3{,}99 \pm 0{,}01)\times10^{-2}$ m and diameter $d = (3{,}275 \pm 0{,}001)\times10^{-2}$ m. The mass m and density ρ of the cylinder are shown in the **Table 1**.

Table 1 The mass and density of the cylinder.

Material	Mass m (kg)	Density ρ (kg/m^3)
Brass	$(2.7158 \pm 0.0002)\times10^{-1}$	(8,062.9 ± 20.6)
Stainless steel	$(2.5112 \pm 0.0002)\times10^{-1}$	(7,455.5 ± 19.1)
Iron	$(2.3798 \pm 0.0002)\times10^{-1}$	(7,065.4 ± 18.1)
Aluminum	$(0.8612 \pm 0.0002)\times10^{-1}$	(2,556.8 ± 6.6)

Tools

The hardware used in this study is a laptop (RAM 4 GB, OS Ms. Windows 7 home premium 32 bit, Intel Core 3), Canon EOS 600D camera with 50 fps (frame per second) which is a tool for making video recordings of the motion of rolling a cylinder in water, the O'haus 3-arm scale which is a cylinder mass weighing device, the O'haus PA 214 digital scale which is a tool for weighing the mass of water that comes out of the aquarium. The software used in this research is Logger Pro 3.2 is a tool for processing video to get time, speed, and position data experimentally.

Procedure

Water is introduced into the aquarium and left for 24 h to achieve thermal equilibrium and to remove trapped air bubbles. The cylinder was also immersed in water at least 24 h prior to the actual experiment. The cylinder was removed using pliers under the water surface in the aquarium, and there were no visible bubbles sticking to the solid cylinder.

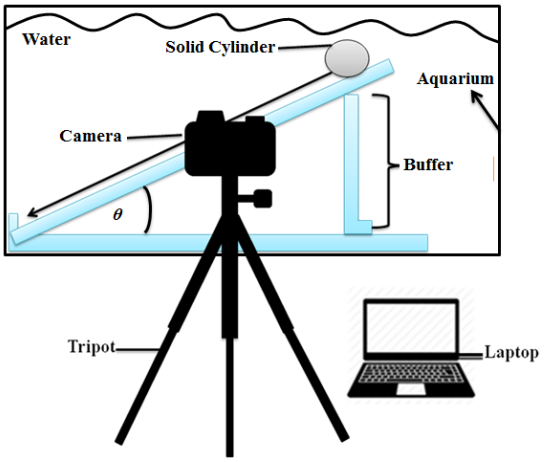

Figure 2 Arrangement of solid cylinder motion data collection tool on an inclined plane in water.

Doing a recording using the camera when a solid cylinder begins to be released on an inclined plane trajectory in the water with variations in tilt angle and density variation. Save recorded videos in a folder for analysis using the Logger Pro software. Repeats recording the motion of a solid cylinder on an inclined plane in water with 7 different tilt angles and 4 different densities of the solid cylinder.

Data analysis

Determine the value of the drag coefficient using Eq. (3) and the density coefficient using Eq. (6). The drag coefficient is calculated using the fitting approach. The data used is a linear function between the squares of the terminal velocity (v_T^2) to the angle of inclination of the plane θ. After that, record the motion of solid cylinders for each solid cylinder, 7 kinds of videos with variations in tilt angle and density variation of solid cylinders, then track the motion of solid cylinders in the video using Logger Pro software, so that data is obtained v_T, data v_T obtained then processed in Microsoft Excel 2007 to get a graph of the relationshipv_T^2 against sin θ. Analysis of experimental data by adjusting the relationship graph v_T^2 against sin θ. The event of a solid cylinder rolling on an inclined plane in the water is a straight motion event that changes regularly, so the data fitting approach used is a linear function. Data fitting aims to obtain the slope value of the relationship graph v_T^2 against sin θ. After obtaining the gradient value from each relationship graph, then the value of the inhibition coefficient is determined by Eq. (3) and when the cylinder rolls on an inclined plane in the water, water comes out of the aquarium so that mass increases. the coefficient can be calculated using Eq. (6). After obtaining the value of the drag coefficient, the additional mass coefficient, the density ratio value of the solid cylinder, the value of time changes and the value of the diameter of the solid cylinder, a solution of nonlinear cylinder motion on an inclined plane in the water numerically will be carried out with Eq. (7). Compared with the solution of cylindrical motion on an inclined plane in the water experimentally obtained from the results of the video tracking from logger pro.

Results and discussion

The drag coefficients of the investigated cylinder shown in **Figure 3** was carried using the methods and the computer programme described above. The drag coefficient on the cylindrical material which affects the terminal velocity is analyzed in this paper.

Drag coefficient

In calculating the coefficient value drag C_D first calculate the slope value of the graph α relationship v_T^2 vs sin θ in Eq. (4) for all cylindrical materials. Relationship graph v_T^2 vs sin θ for each cylinder with various angles 10, 13, 15, 18, 20, 23, 25 ° at a fixed distance 0.95 m as follows:

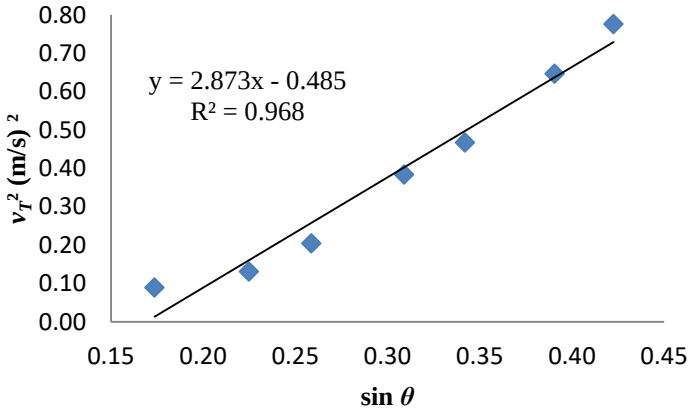

(a)

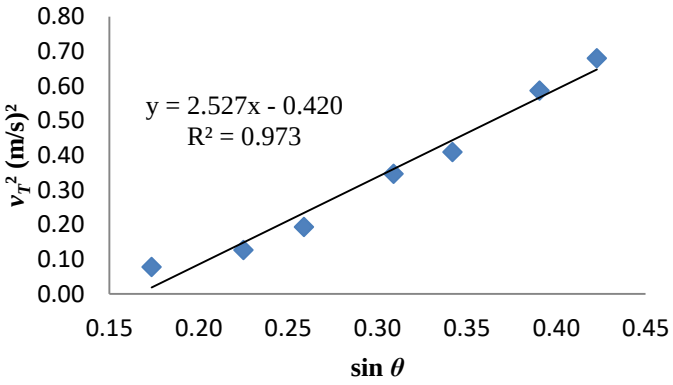

(b)

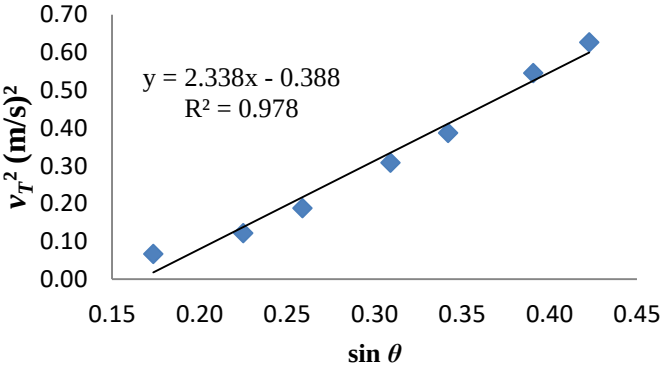

(c)

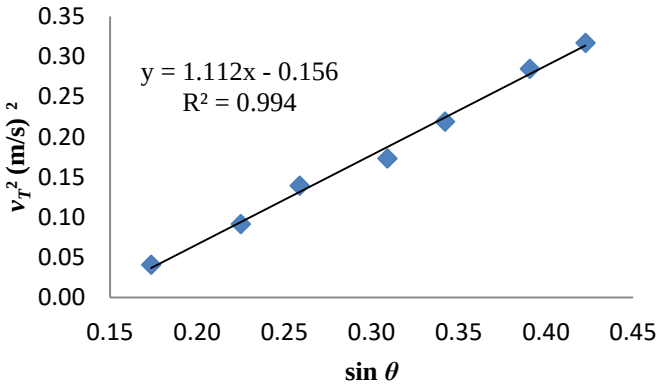

(d)

Figure 3 Relationship graph vT2 vs sin θ for: (a) brass cylinders; (b) stainless steel cylinder; (c) iron cylinder, and (d) aluminum cylinder.

From **Figures 3(a) - 3(d)** the values obtained are: For a brass cylinder the terminal velocity at an angle of 10 ° is 0.29952 m/s, an angle of 13 ° is 0.36264 m/s, an angle of 15 ° is 0.45218 m/s, an angle of 18 ° is 0.61970 m/s, 20 ° angle is 0.68398 m/s, 23 ° angle is 0.80412 m/s and 25 ° angle is 0.88079 m/s. Furthermore, for stainless steel cylinder the terminal velocity at 10 ° angle is 0.2786 m/s, 13 ° angle is 0.3557 m/s, 15 ° angle is 0.4397 m/s, 18 ° angle is 0.5885 m/s, 20 ° angle is 0.6400 m/s, 23 ° angle is 0.7662 m/s and 25 ° angle is 0.8245 m/s. For iron cylinder terminal velocity at 10 ° angle is 0.2583 m/s, 13 ° angle is 0.3494 m/s, 15 ° angle is 0.4338 m/s, 18 ° angle is 0.5551 m/s, 20 ° angle is 0.6223 m/s, 23 ° angle is 0.7384 m/s and 25 ° angle is 0.7917 m/s. In addition, for aluminum cylinders, the terminal velocity at an angle of 10 ° is 0.220 m/s, an angle of 13 ° is 0.3021 m/s, an angle of 15 ° is 0.3732 m/s, an angle of 18 ° is 0.4160 m/s, an angle of 20 ° is 0.4160 m/s. 0.4681 m/s, 23 ° angle is 0.5334 m/s and 25 ° angle is 0.5631 m/s. From the terminal velocity values for all cylindrical materials, it can be seen that the aluminum cylinder experienced the most significant speed deceleration, this was due to the rolling motion of the cylinder in the water being slowed by the buoyant force of water because the density of the cylinder was almost the same as the density of water.

By using the slope value of each cylinder, the C_D drag coefficient value can be calculated by entering the graph slope value into Eq. (4) for all cylinder materials, so that the C_D drag coefficient value is obtained in **Table 2**.

Table 2 Drag coefficient C_D cylinder.

Material	Slope of the graph α	Drag coefficient C_D
Brass	(2.8730 ± 0.3996)	(1.2388 ± 0.1724)
Stainless steel	(2.5270 ± 0.3208)	(1.2873 ± 0.1635)
Iron	(2.3384 ± 0.2676)	(1.3071 ± 0.1497)
Aluminum	(1.1124 ± 0.0666)	(0.7052 ± 0.0424)

From **Table 2** it can be seen that the slope value obtained from fitting the squared terminal velocity data to the angle variation is the most important parameter in obtaining the drag coefficient value for each cylinder material. The value of the drag coefficient of iron is the largest and the value of the drag coefficient of aluminum is the smallest. The relative error of drag coefficient for brass cylinder material is 13.92 %, stainless steel is 12.70 %, iron is 11.45 % and aluminum is 6.01 %. From the relative error, the value of the drag coefficient obtained is good, although there is an increase in error but it is not significant. In addition, the value of the drag coefficient also represents the magnitude of the drag force that works when each cylinder rolls in the water, which can cause laminar or turbulent water flow. This is due to the effect of the density of each cylinder material when in the water due to buoyancy [59].

Reynold number R_e

The Reynold number coefficient is calculated by Eq. (5) for each cylinder in **Table 3**.

Table 3 Reynold's number of brass and stainless steel cylinders.

θ (°)	v	R_e brass	R_e stainless steel	R_e iron	R_e alumunium
10	v_{min}	(156.0 ± 0.0)	(31.9 ± 0.0)	(349.0 ± 0.1)	(399.9 ± 0.1)
	v_{max}	(9,530.9 ± 2.3)	(13,108.9 ± 3.2)	(7,075.6 ± 1.7)	(5,440.4 ± 1.3)
13	v_{min}	(428.8 ± 0.1)	(503.6 ± 0.1)	(224.0 ± 0.1)	(471.7 ± 0.1)
	v_{max}	(17,981.8 ± 4.4)	(17,379.8 ± 4.2)	(12,890.9 ± 3.1)	(10,667.7 ± 2.6)
15	v_{min}	(1,187.4 ± 0.3)	(273.1 ± 0.1)	(472.4 ± 0.1)	(300.6 ± 0.1)
	v_{max}	(12,888.6 ± 3.1)	(15,021.8 ± 3.7)	(16,704.3 ±4.1)	(6,207.5 ± 1.5)
18	v_{min}	(443.1 ± 0.1)	(343.9 ± 0.1)	(783.3 ± 0.2)	(935.7 ± 0.2)
	v_{max}	(14,758.1 ± 3.6)	(20,992.5 ± 5.1)	(21,974.5 ± 5.4)	(9,890.7 ± 2.4)
20	v_{min}	(521.2 ± 0.1)	(420.6 ± 0.1)	(747.9 ± 0.2)	(383.7 ± 0.1)
	v_{max}	(15,803.3 ± 3.9)	(21,305.5 ± 5.2)	(24,718.2 ± 6.0)	(13,792.8 ± 3.4)
23	v_{min}	(8.9 ± 0.0)	(1,068.5 ± 0.3)	(1,068.5 ± 0.1)	(1,197.2 ± 0.3)
	v_{max}	(22,182.1 ± 5.4)	(22,173.2 ± 5.4)	(23,919.9 ± 5.8)	(12,125.9 ± 3.0)
25	v_{min}	(146.1 ± 0.0)	(782.4 ± 0.2)	(93.7 ± 0.0)	(242.8 ± 0.1)
	v_{max}	(25,553.9 ± 6.2)	(52,508.0 ± 12.8)	(26,607.6 ± 6.5)	(11,353.1 ± 2.8)

From **Table 3** it can be seen that the Reynolds number of brass cylinders (156.0 - 25,553.9) and stainless steel cylinders (31.9 - 52,508.0) is less than 3×105, so the flow is laminar [58], the Reynolds number of iron cylinders (349.0 - 26,607.6) and aluminum cylinders (399.9 - 11,353.1) is less than 3×105, so the flow is laminar [58]. Overall there are 7 variations of the slope angle data for 4 types of cylindrical material with a Reynolds number value of 31.9 < Re < 52,508.0, the data is separated into different sub-groups depending on the type of cylinder material. **Tables 2** and **3** show the effect of the drag coefficient on the resulting Reynolds number. It is seen that when the value of the drag coefficient increases, the Reynolds number increases. As the Reynolds number increases, the water flow rate also increases, but still without a turbulent flow trend. The flow conditions seen are laminar for all types of cylindrical materials rolling in the water. So, in this study, it is necessary to test it with a cylindrical trajectory in the form of a tube and record it using a high-speed camera with a much larger frame so that new data can be obtained as a comparison from this study.

Conclusions

In this study, the fluid dynamics of the cylindrical drag on an inclined plane in water was measured experimentally. The data reported in this study include 7 variations of angle and 4 variations of cylinder density. Overall, this study includes a slope angle of 10, 13, 15, 18, 20, 23, and 25 ° with the brass drag coefficient 1.2388, stainless steel drag coefficient 1.2873, iron drag coefficient 1.3071, aluminum drag coefficient 0.7052 and Reynolds number of brass cylinders (156.0 - 25,553.9), stainless steel cylinders (31.9 - 52,508.0), iron cylinders (349.0 - 26,607.6) and aluminum cylinders (399.9 - 11,353.1) is less than 3×105, which means the water is in a laminar state. In addition, the value of the terminal velocity achieved is determined by the angle of inclination of the plane and the density of the material which will affect the magnitude of the drag force based on the linear regression Eqs. (2) - (4). The greater the angle of inclination of the plane, the greater the terminal velocity achieved. In addition, the resistance acting on the cylinder when it is rolling on an inclined plane in water is another external force (besides the drag coefficient) that hinders the cylinder when it is rolling. In addition, the cylinder motion is also not perfectly linear because there is a force from the side of the track and the cylinder moves slightly zigzag in 1-D motion. The results obtained in this study can be used for broader scientific problems, especially the potential for hydrometeorological and sedimentation disasters.

Acknowledgements

This research was supported by the STKIP Muhammadiyah OKU Timur and WANI (Wave, Vibration and Fluid) Laboratory, Master Program of Physics Education, Ahmad Dahlan University, Yogyakarta, Indonesia.

References

[1] RP Chhabra, M Kumar and P Rishitosh. Drag on spheres in rolling motion in inclined smooth tubes filled with incompressible liquids. *Powder Tech*. 2000; **113**, 114-8.
[2] R Clift, J Grace and ME Weber. *Drops and particles*. Academic, New York, 1978.
[3] R Martino, A Paterson and MF Piva. Experimental and analytical study of themotion of a sphere falling along an inclined plane in still water. *Powder Tech*. 2015; **283**, 227-33.
[4] RP Chhabra. *Bubbles, drops and particles, in non-newtonian fluids*. CRC Press, Florida,1993.
[5] RP Chhabra and JM Ferreira. An analytical study of the motion of a sphere rolling down a smooth inclined plane in an incompressible Newtonian fluid. *Powder Tech*. 1999; **104**, 130-8.
[6] B Zeinali and J Ghazanfarian. Turbulent flow over partially superhydrophobic underwater structures: The case of flow over sphere and step. *Ocean Eng*. 2020; **195**, 106688.
[7] EA Ashmawy. Wall effects on a rigid sphere moving perpendicular to a plane wall in a couple stress fluid filling a half-space. *Eur. J. Mech. B Fluid* 2019; **74**, 380-8.
[8] JT Jeong. Axisymmetric stokes flow around a sphere translating along the axis of a circular cylinder. *Eur. J. Mech. B Fluid* 2019; **77**, 252-8.
[9] G Mishra, SA Patel and RP Chhabra. Pulsatile flow of power-law fluids over a sphere: Momentum and heat transfer characteristics. *Powder Tech*. 2020; **360**, 789-817.
[10] TH Shehadeh and EA Ashmawy. Interaction of two rigid spheres translating collinearly in a couple stress fluid. *Eur. J. Mech. B Fluid* 2019; **78**, 284-90.
[11] Z Peng, K Galvin and E Doroodchi. Influence of inclined plates on flow characteristics of a liquid-solid fluidised bed: A CFD-DEM study. *Powder Tech*. 2019; **343**, 170-84.
[12] SS Tiwari, E Pal, S Bale, N Minocha, AW Patwardhan, K Nandakumar and JB Joshi. Flow past a single stationary sphere, 2. Regime mapping and effect of external disturbances. *Powder Tech*. 2020; **365**, 215-43.
[13] AT Sholagberu, MR Mustafa, KW Yusof and AM Hashim. Geostatistical based susceptibility mapping of soil erosion and optimization of its causative factors: a conceptual framework. *J. Eng. Sci. Tech*. 2017; **12**, 2880-95.
[14] GG Dogan, A Annunziato, R Hidayat, S Husrin, G Prasetya, W Kongko, A Zaytsev, E Pelinovsky, F Imamura and AC Yalciner. Numerical simulations of December 22, 2018 Anak Krakatau Tsunami and examination of possible submarine landslide scenarios. *Pure Appl. Geophys*. 2021; **178**, 1-20.
[15] T Zengaffinen, F Løvholt, GK Pedersen and A Muhari. Modelling 2018 Anak Krakatoa flank collapse and Tsunami: Effect of landslide failure mechanism and dynamics on Tsunami generation. *Pure Appl. Geophys*. 2020; **177**, 2493-516.
[16] Syamsidika, Benazira, M Umara, G Margaglio and A Fitrayansyaha. Post-tsunami survey of the 28 September 2018 tsunami near Palu Bay in Central Sulawesi, Indonesia: Impacts and challenges to coastal communities. *Int. J. Disast. Risk Reduction* 2019; **38**, 101229.
[17] J Wanga, SN Ward and L Xiaoa. Tsunami squares modeling of landslide generated impulsive waves and its application to the 1792 Unzen-Mayuyama mega-slide in Japan. *Eng. Geol*. 2019; **256**, 121-37.
[18] R Brackenridge, U Nicholson, B Sapiie, D Stow and DR Tappin. Indonesian throughflow as a preconditioning mechanism for submarine landslides in the Makassar Strait. *Geol. Soc. Spec. Publ.* 2020; **500**, 195-217.
[19] T Giachetti, R Paris, K Kelfoun and B Ontowirjo. Tsunami hazard related to a flank collapse of Anak Krakatau Volcano, Sunda Strait, Indonesia. *Geol. Soc. Spec. Publ.* 2012; **361**, 79-90.
[20] FD Traglia, T Nolesinia, L Solaria, A Ciampalini, W Frodella, D Steria, B Allotta, A Rindi, L Marini, N Monni, E Galardi and N Casaglia. Lava delta deformation as a proxy for submarine slope instability. *Earth Planet. Sci. Lett*. 2018; **488**, 46-58.

[21] J Karstens, C Berndt, M Urlaub, SFL Watt, A Micallef, M Ray, I Klaucke, S Muff, D Klaeschen, M Kühn, T Roth, C Böttner, B Schramm, J Elger and S Brune. From gradual spreading to catastrophic collapse-Reconstruction of the 1888 Ritter Island volcanic sector collapse from high-resolution 3D seismic data. *Earth Planet. Sci. Lett*. 2019; **517**, 1-13.

[22] M Carvajal, C Araya-Cornejo, I Sepúlveda, D Melnick and JS Haase. Nearly instantaneous tsunamis following the MW 7.5 2018 Palu earthquake. *Geophys. Res. Lett*. 2019; **46**, 5117-26.

[23] H Takagi, MB Pratama, S Kurobe, M Esteban and R Aránguiz. Analysis of generation and arrival time of landslide tsunami to Palu City due to the 2018 Sulawesi Earthquake. *Landslides* 2019; **16**, 983-91.

[24] R Williams, P Rowley and MC Garthwaite. Reconstructing the Anak Krakatau flank collapse that caused the December 2018 Indonesian tsunami. *Geology* 2019; **47**, 973-6.

[25] A Perttu, C Caudron, D Assink J, D Metz, D Tailpied, B Perttu, C Hibert, D Nurfiani, C Pilger, M Muzli, D Fee, L Andersen O and B Taisne. Reconstruction of the 2018 tsunamigenic flank collapse and eruptive activity at Anak Krakatau based on eyewitness reports, seismo-acoustic and satellite observations. *Earth Planet. Sci. Lett*. 2020; **541**, 116268.

[26] S Viroulet, A Sauret and O Kimmoun. Tsunami generated by a granular collapse down a rough inclined plane. *Europhys. Lett*. 2014; **105**, 34004.

[27] R Delannay, A Valance, A Mangeney, O Roche and P Richard. Granular and particle-laden flows: From laboratory experiments to field observations. *J. Phys. Appl. Phys*. 2017; **50**, 053001.

[28] M Bursik, A Patra, EB Pitman, C Nichita, JL Macias, R Saucedo and O Girina. Advances in studies of dense volcanic granular flows. *Rep. Progr. Phys*. 2005; **68**, 271-301.

[29] S Abadie, J Harris, S Grilli and R Fabre. Numerical modeling of tsunami waves generated by the ank collapse of the Cumbre Vieja Volcano (La Palma, Canary Islands): Tsunami source and near field effects. *J. Geophys. Res.* 2012; **117**, C05030.

[30] L Verrucci, P Tommasi, D Boldini, A Graziani and T Rotonda. Modelling the instability phenomena on the NWflank of Stromboli Volcano (Italy) due to lateral dyke intrusion. *J. Volcanol. Geoth. Res*. 2019; **371**, 245-62.

[31] R Omira, GG Dogan, R Hidayat, S Husrin, G Prasetya, A Annunziato, C Proietti, P Probst, MA Paparo, M Wronna, A Zaytsev, P Pronin, A Giniyatullin, PS Putra, D Hartanto, G Ginanjar, W Kongko, E Pelinovsky and AC Yalciner. The September 28th, 2018, Tsunami in Palu-Sulawesi, Indonesia: A post-event field survey. *Pure Appl. Geophys*. 2019; **176**, 1379-95.

[32] HW Lewis. Calibration of rolling ball viscometer. *Anal. Chem.* 1953; **25**, 507-8.

[33] MS Medania and MA Hasan. Viscosity of organic liquids at elevated temperatures and the corresponding vapour pressures. *Can. J. Chem. Eng.* 1977; **55**; 203-9.

[34] MA Hasan. Wall effects on the motion of a rolling sphere in a closely fitting tube. *Chem. Eng. J*. 1986; **33**, 97-101.

[35] RJ Garde, S Sethuraman and LH Blanche. Variation of the drag coefficient of a sphere rolling along a boundary. *Houille Blanche, La* 1969; **7**, 727-32.

[36] R Ariefka and Y Pramudya. The study of hollow cylinder on inclined plane to determine the cylinder moment of inertia. *J. Phys. Conf*. 2019; **1170**, 012081.

[37] S Zhao, HC Schneider and M Kamlah. An experimental method to measure the friction coefficients between a round particle and a flat plate. *Powder Tech*. 2020; **361**, 983-9.

[38] SK Samantaray, BK Rout, SS Mohapatra and B Munshi. Newtonian flow past a hollow frustum in vertical and inclined plane: An experimental observation for terminal velocity and drag coefficient. *Powder Tech*. 2018; **326**, 114-22.

[39] EA Molaei, AB Yu and ZY Zhou. Particle scale modelling of mixing of ellipsoids and spheres in gas-fluidized beds by a modified drag correlation. *Powder Tech*. 2019; **343**, 619-28.

[40] EA Molaei, AB Yu and ZY Zhou. Particle scale modelling of solid flow characteristics in liquid fluidizations of ellipsoidal particles. *Powder Tech*. 2018; **338**, 677-91.

[41] AA Zaidi. Granular drag force during immersion in dry quicksand. *Powder Tech*. 2020; **364**, 986-93.

[42] C Béguin, S Étienne and MJ Pettigrew. Effect of dispersed phase fraction on the drag coefficient of a droplet or a bubble in an idealized two-phase flow. *Eur. J. Mech. B Fluid*. 2017; **65**; 339-49.

[43] S Chamoli, T Tang, P Yu and R Lu. Effect of shape modification on heat transfer and drag for fluid flow past a cam-shaped cylinder. *Int. J. Heat Mass Tran*. 2019; **131**, 1147-63.
[44] L Qingling, T Shouceng, S Zhonghou, X Zhengming and P Zhaoyu. A new equation for predicting settling velocity of solid spheres in fiber containing power-law fluids. *Powder Tech*. 2018; **329**, 270-81.
[45] D Zhang, S Hua, R Zhanga, X Jianga, C Zhanga, H Yina, C Wange and X Qub. Development of an explicit formula for predicting the drag coefficients of equiaxed dendrites. *Comput. Mater. Sci*. 2020; **172**, 109319.
[46] TR Jayawickrama, NEL Haugen, MU Babler, MA Chishty and K Umeki. The effect of Stefan flow on the drag coefficient of spherical particles in a gas flow. *Int. J. Multiphas. Flow* 2019; **117**, 130-37.
[47] A Jetly, IU Vakarelski, Z Yang and ST Thoroddsen. Giant drag reduction on Leidenfrost spheres evaluated from extended freefall trajectories. *Exp. Therm. Fluid Sci*. 2019; **102**, 181-8.
[48] H Jin, H Wang, Z Wu, Z Ren and Z Ou. Numerical investigation on drag coefficient and flow characteristics of two biomass spherical particles in supercritical water. *Renew. Energ*. 2019; **138**, 11-7.
[49] W Kim, H Lee, J Lee, D Jung and H Choi. Flow over a ski jumper in flight: Prediction of the aerodynamic force and flight posture with higher lift-to-drag ratio. *J. Biomech*. 2019; **89**, 78-84.
[50] VA Shuvalov, NB Gorev, NA Tokmak and YP Kuchugurnyi. Drag on a spacecraft produced by the interaction of its magnetic field with the Earth's ionosphere. Physical modelling. *Acta Astronautica* 2019; **166**, 41-51.
[51] S Li, J Yang and Q Wang. Large eddy simulation of flow and heat transfer past two side-by-side spheres. *Appl. Therm. Eng*. 2017; **121**, 810-9.
[52] WRA Goossens. Review of the empirical correlations for the drag coefficient of rigid spheres. *Powder Tech*. 2019; **352**, 350-9.
[53] DJ Tritton. *Physical fluid dynamics*. Springer Dordrecht, New York, 1977.
[54] CA Ramírez. Summary of frictional drag coefficient relationships for spheres: Evolving solution strategies applied to an old problem. *Chem. Eng. Sci*. 2017; **168**, 339-43.
[55] Y Chen and CR Müller. Development of a drag force correlation for assemblies of cubic particles: The effect of solid volume fraction and reynolds number. *Chem. Eng. Sci*. 2018; **192**, 1157-66.
[56] VD Sarli, E Danzi, L Marmo, R Sanchirico and AD Benedetto. CFD simulation of turbulent flow field, feeding and dispersion of non-spherical dust particles in the standard 20 L sphere. *J. Loss Prev. Process Indust*. 2019; **62**, 103983.
[57] F Marchelli, Q Hou, B Bosio, E Arato and A Yu. Comparison of different drag models in CFD-DEM simulations of spouted beds. *Powder Tech*. 2020; **360**, 1253-70.
[58] A Bahatmaka and DJ Kim. Numerical approach for the traditional fishing vessel analysis of resistance by cfd. *J. Eng. Sci. Tech*. 2019; **14**, 207-17.
[59] BHMA Mahmoud. *Particle dispersion and deposition in simulant nuclear waste slurries using novel ultrasonic techniques*. Master Thesis. University of Leeds, England.